Featured in Physics

Emergence of Isotropy and Dynamic Scaling in 2D Wave Turbulence in a Homogeneous Bose Gas

Maciej Gałka,[1,*] Panagiotis Christodoulou,[1] Martin Gazo,[1] Andrey Karailiev,[1] Nishant Dogra,[1] Julian Schmitt,[1,2] and Zoran Hadzibabic[1]

[1] *Cavendish Laboratory, University of Cambridge, J. J. Thomson Avenue, Cambridge CB3 0HE, United Kingdom*
[2] *Institut für Angewandte Physik, Universität Bonn, Wegelerstraße 8, 53115 Bonn, Germany*

(Received 28 May 2022; revised 24 August 2022; accepted 14 September 2022; published 4 November 2022)

We realize a turbulent cascade of wave excitations in a homogeneous 2D Bose gas and probe on all relevant time and length scales how it builds up from small to large momenta, until the system reaches a steady state with matching energy injection and dissipation. This all-scales view directly reveals the two theoretically expected cornerstones of turbulence formation—the emergence of statistical momentum-space isotropy under anisotropic forcing and the spatiotemporal scaling of the momentum distribution at times before any energy is dissipated.

DOI: 10.1103/PhysRevLett.129.190402

Turbulence is a multiscale phenomenon that is still not understood on a microscopic level, but is believed to generically feature cascades of excitations across different length scales [1–3]. When Richardson introduced the concept of a turbulent cascade a century ago [1], he posited that energy injected into a fluid at a large length scale flows without loss through momentum space until it is dissipated at some small length scale. This is now known as a direct cascade, and the concept has been extended to an inverse one [4], from small to large length scales.

In a fully developed steady state, with matching energy injection (at one length scale) and dissipation (at another), turbulence is commonly manifested in stationary power-law spectra of system-dependent quantities like energy [5] or enstrophy [4,6]. Such spectra have been observed in a variety of contexts [5–9], ranging from ocean waves [8] to financial markets [7]. However, little is established experimentally about how such nonequilibrium steady states emerge, starting from an equilibrium system.

In this Letter, we observe this emergence for a direct wave cascade in a homogeneous two-dimensional (2D) atomic Bose gas [10,11]. Compared to earlier work on 3D wave turbulence in a homogeneous Bose gas [12], our geometry allows us to directly view the system on all relevant length scales, from the large one where we inject energy by an oscillating force to the small one where it is eventually dissipated. Our Letter also complements studies of the inverse energy cascade associated with vortex turbulence in 2D Bose gases [13,14] and opens possibilities for further research, ranging from the interplay of wave and vortex turbulence [15] to quantum simulation of processes believed to have taken place in the early Universe [16].

The two key phenomena theoretically associated with the birth of direct-cascade wave turbulence are outlined in Fig. 1(a). First, according to this picture, even though the continuous energy injection at a large length scale (small wave number $k = |\mathbf{k}|$) is anisotropic, beyond a sufficiently large k the cascade is statistically isotropic; such isotropy is believed to emerge in systems that, like our trapped gas, carry no net momentum [17] (see [18,19] for a more general discussion). The second key phenomenon is dynamic scaling—once the isotropic cascade front $k_{\rm cf}$ forms, it evolves algebraically in time t, as $k_{\rm cf} \propto t^{-\beta}$ (with $\beta < 0$), until it reaches the dissipation scale k_D and a steady state is established. In its wake, $k_{\rm cf}$ leaves an isotropic power-law momentum distribution $n_k(\mathbf{k}) \propto k^{-\gamma}$ [19,20], so the pre-steady-state n_k (at large k) follows the general form of self-similar spatiotemporal (dynamic) scaling,

$$(t/t_0)^{-\alpha} n_k(\mathbf{k}, t) = n_k((t/t_0)^{\beta}\mathbf{k}, t_0), \qquad (1)$$

where t_0 is a reference time and in our case $\alpha = \gamma\beta$ [19,20]. Such scaling, known from classical surface growth [21,22], and also seen in the relaxation dynamics of quantum gases [23–27], is hypothesized to be generic to far-from-equilibrium many-body quantum systems [28,29] and proposed as a way to classify them analogously to equilibrium universality classes.

As outlined in Fig. 1(b), we prepare a quasipure 2D superfluid of ^{39}K atoms in a square optical box trap and drive it anisotropically with a time-periodic force created by a magnetic field gradient along one of the box axes, denoted x [30]. The gas is confined to the x-y plane by a harmonic potential with angular trap frequency ω_z and has chemical potential $\mu = N\hbar^2\tilde{g}/(mL^2)$, where N is the atom number, L is the box size, m is the atom mass, and $\tilde{g} = \sqrt{8\pi m\omega_z/\hbar}a$ [31,32], where a is the 3D s-wave scattering length, which we tune using a Feshbach resonance; for our

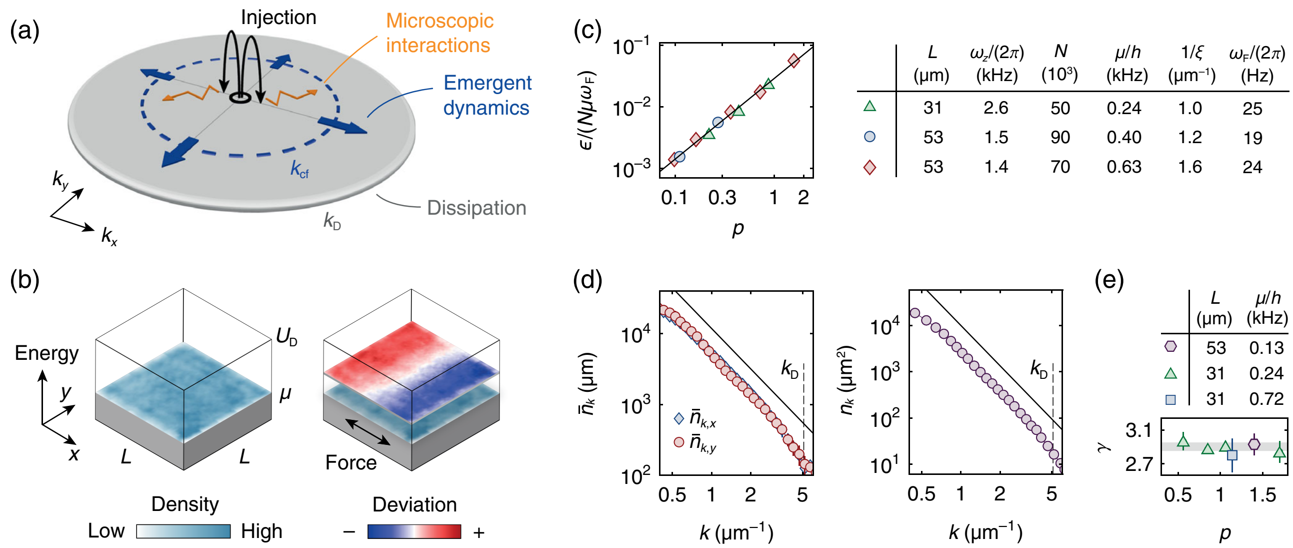

FIG. 1. Direct wave cascade in a 2D quantum gas. (a) Generic momentum-space picture of emergent isotropy and dynamic scaling. Anisotropic energy injection at a small wave number k (black) and microscopic interactions (orange) lead to an isotropic cascade (blue), with the cascade front evolving as $k_{\mathrm{cf}} \propto t^{-\beta}$ (where t is time and $\beta < 0$) until it reaches the dissipation scale k_D and a steady state is established. (b) Our experiment. Left: we start with a homogeneous 2D superfluid of N atoms with chemical potential μ in a square box trap of size L (here 53 μm) and depth U_D, which sets $k_D \propto \sqrt{U_D}$. Right: a spatially uniform force $F = F_0 \sin(\omega_F t)$ along x resonantly injects energy into a phonon mode with wave vector $\mathbf{k}_F = (\pi/L, 0)$, visualized using PCA. (c)–(e) Universal steady-state features. (c) The energy-injection rate ϵ scaled by $N\mu\omega_F$ for different system parameters. The solid line shows $\epsilon/(N\mu\omega_F) \propto p^{1.31(3)}$, where $p = F_0 L/\mu$. (d) Steady-state momentum distributions seen in TOF for $p = 0.85$ and system parameters as for the green triangles in (c). Left: line-integrated distributions parallel ($\bar{n}_{k,x}$) and perpendicular ($\bar{n}_{k,y}$) to the drive; right: azimuthally averaged $n_k(k)$. The solid lines show $n_k \propto k^{-\gamma}$ and $\bar{n}_{k,x(y)} \propto k^{-\gamma+1}$, with $\gamma = 2.9$. (e) Exponent γ for different experimental parameters; shaded region shows $\gamma = 2.90(5)$.

typical system parameters, see the legend in Fig. 1(c). The spatially uniform driving force, $F = F_0 \sin(\omega_F t)$, with $\omega_F = c\pi/L$, where $c = \sqrt{\mu/m}$ is the speed of sound, resonantly injects energy into a longest-wavelength phonon mode, with wave vector $\mathbf{k}_F = (\pi/L, 0)$. Our energy-injection scale is thus set by the system size, $k_F = \pi/L \lesssim 0.1\ \mu\mathrm{m}^{-1}$, while the dissipation scale $k_D = \sqrt{2mU_D/\hbar^2} \approx 5\ \mu\mathrm{m}^{-1}$ is set by the trap depth U_D; the energy is dissipated from the system by particles with energy larger than U_D leaving the trap [33,34]. Between k_F and k_D, the nature of excitations changes from phonons to particlelike matter waves at $k = 1/\xi$, where $\xi = L/\sqrt{\tilde{g}N} \sim 1\ \mu$m is the 2D healing length [32].

We first summarize the universal features of our energy injection [Fig. 1(c)] and the resulting steady-state turbulence [Figs. 1(d) and 1(e)] and then study how such a steady state gets established (Figs. 2 and 3). To probe the gas on all length scales from k_F to k_D, we use three complementary tools: (i) using principal component analysis (PCA) [35,36], we directly visualize the dynamics of the low-lying ($k \sim k_F$) discrete quantum states; (ii) with time-of-flight (TOF) expansion, we study the emergent statistical behavior at large k; and (iii) using Bragg spectroscopy [37,38], we bridge the k-space gap between these measurements.

To measure the energy flux ϵ injected at $\mathbf{k}_F$ (averaged over half a drive period), we monitor the periodic displacement of the cloud's center of mass (c.m.), which is proportional to the density modulation due to the phonon excitation at $\mathbf{k}_F$ [see Fig. 1(b)] [30]. Specifically, $\epsilon = N F_0 v_0/2$, where v_0 is the amplitude of the c.m. speed. Defining the dimensionless flux $\epsilon/(N\mu\omega_F) = p v_0/(2\pi c)$, where $p = F_0 L/\mu$ is the dimensionless drive strength [12], we find that it follows a universal curve, $\propto p^{1.31(3)}$ [Fig. 1(c)]. This scaling is in contrast with linear response (where $v_0 \propto F_0$, so $\epsilon \propto p^2$) and agrees with $\epsilon \propto p^{4/3}$ for a nonlinear transfer of energy to higher-lying excitations, as previously observed in 3D for a single interaction strength [39].

For sufficiently strong drives, $p \gtrsim 0.5$ (corresponding to $v_0/c \gtrsim 0.15$), and at sufficiently long times, in TOF we observe steady-state power-law distributions such as those shown in Fig. 1(d) for $p = 0.85$ and $t = 5 \times 2\pi/\omega_F$. The line-integrated distributions parallel and perpendicular to the drive, $\bar{n}_{k,x(y)}(k_{x(y)}) = \int dk_{y(x)} n_k(k_x, k_y)$, are essentially identical, implying an isotropic n_k. Note, however, that due to finite-size effects, these measurements are not accurate for $k \lesssim 0.6\ \mu\mathrm{m}^{-1}$ (see Supplemental Material [40]). We also show the (azimuthally averaged) radial distribution $n_k(k)$, from which we extract $\gamma \approx 2.9$ (solid line). As shown in Fig. 1(e), γ is robust under changes of the system

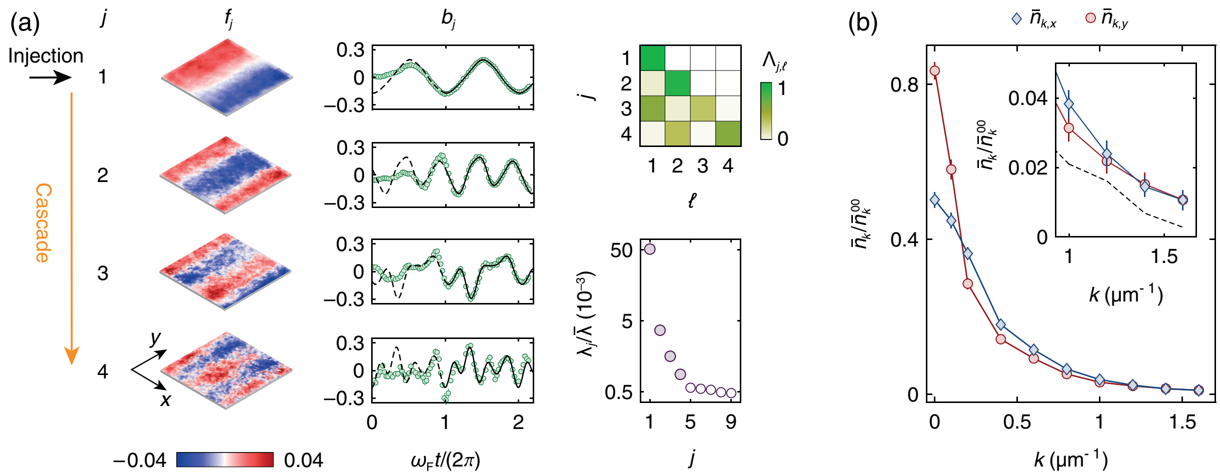

FIG. 2. From low-k anisotropy to high-k isotropy. (a) PCA decomposition of the *in situ* density modulations, for $p = 0.6$. The spatial structures $f_j(x, y)$ of the first four modes show excitations only along the drive direction x. The temporal fits, $b_j(t) = \sum_{\ell=1}^{4} B_{j,\ell} \cos(\ell\omega_F t + \phi_{j,\ell})$ for $t > 2\pi/\omega_F$ (solid lines, with the dashed ones showing extrapolations to shorter t), give the harmonic weights $\Lambda_{j,\ell} = B_{j,\ell}^2/(\sum_{\ell=1}^{4} B_{j,\ell}^2)$. The normalized PCA eigenvalues $\lambda_j/\bar{\lambda}$ are also shown for the next five modes (open circles), which do not show any clear structures. (b) Emergence of isotropy seen in Bragg spectroscopy, for $p = 0.85$ and $t = 2\pi/\omega_F$. Here $\bar{n}_{k,x}(k)$ and $\bar{n}_{k,y}(k)$ are normalized by their common value $\bar{n}_k^{00}$, measured for $k = 0$ and $t = 0$. The emergence of isotropy is seen in the convergence of the two curves for $k \gtrsim 1/\xi = 1.0\ \mu\text{m}^{-1}$; in the inset (enlarged at high k), the dashed line indicates distributions measured with similar error bars for $p = 0$.

parameters, including the box size and the drive strength; from different measurements (always fitting in the range 1.5–3 μm^{-1}) we get a combined estimate $\gamma = 2.90(5)$.

To trace how such a steady state gets established, we start with the onset of the cascade at low k, by studying *in situ* the spatiotemporal modulations of the gas density n [Fig. 2(a)]; here we use our larger, 53-μm box, with parameters as for the red diamonds in Fig. 1(c) and $p = 0.6$, while below for Bragg and TOF measurements we use a 31-μm box with all parameters as in Fig. 1(d) [40]. Using PCA, we decompose $n(x, y, t)$ in an unbiased way as $\sqrt{\bar{\lambda}}\bar{f}(x, y) + \sum_{j=1}^{J-1} \sqrt{\lambda_j} f_j(x, y) b_j(t)$, with orthonormal $\{f_j(x, y)\}$ and $\{b_j(t)\}$, and J equal to the number of different times for which we measure n. Here $\bar{f}$ is the normalized time-averaged density profile and f_j are the principal components of the modulations $\Delta n(x, y, t)$, with eigenvalues λ_j decreasing with increasing j, and $\sum_{j=1}^{J-1} \lambda_j/\bar{\lambda} = \langle(\Delta n)^2\rangle/\langle n\rangle^2$, where $\langle \ldots \rangle$ denotes an average over both space and time. For weak modulations, f_j directly visualize the wave functions of the underlying excitations through interference with the quasiuniform condensate.

We find that the first four f_j [see Fig. 2(a)], with f_1 showing the resonantly excited phonon, all closely resemble phonon wave functions with $\mathbf{k} = j\mathbf{k}_F$; here $J = 81$, but the first four modes account for 75% of the total (normalized) density variance $\sum_{j=1}^{80} \lambda_j/\bar{\lambda} = 0.08$, and we do not identify any clear structures in the remaining ones. The directly driven b_1 oscillation at ω_F quickly reaches a steady state, while b_2 oscillates predominantly at $2\omega_F$ and with a discernible delay; b_3 and b_4 show more complex behavior, but for $t > 2\pi/\omega_F$, all four b_j are fitted well by $\sum_{\ell=1}^{4} B_{j,\ell} \cos(\ell\omega_F t + \phi_{j,\ell})$, which gives their harmonic weights $\Lambda_{j,\ell} = B_{j,\ell}^2/(\sum_{\ell=1}^{4} B_{j,\ell}^2)$. The nonlinear cascade naturally results in the appearance of the diagonal terms $\Lambda_{j,j}$, corresponding to $j\mathbf{k}_F$ phonons being created and revealed through interference with the condensate. The prominent off-diagonal ones $\Lambda_{3,1}$ and $\Lambda_{4,2}$ can be partially explained by noting that two-phonon interference also contributes to Δn (e.g., $B_{4,2}$ arising from interference of $\mathbf{k}_F$ and $3\mathbf{k}_F$ phonons); another contribution to $B_{3,1}$ arises from weak off-resonant direct driving of the $3\mathbf{k}_F$ phonon.

Crucially, up to $4k_F$, corresponding to $\approx 0.15/\xi$, all the dynamics are essentially one dimensional. In the presence of a condensate, which makes a three-wave interaction (two phonons combining into a single higher-energy one) the dominant nonlinear process, such absence of cross-directional coupling is indeed theoretically expected for $k \ll 1/\xi$ [46].

To follow the fate of the anisotropy at higher k, we use Bragg spectroscopy, which gives the line-integrated distributions $\bar{n}_{k,x}$ and $\bar{n}_{k,y}$ without any finite-size artifacts. Normalizing $\bar{n}_{k,x}(k)$ and $\bar{n}_{k,y}(k)$ to unity for zero k and t [40], in Fig. 2(b) we show them for $t = 2\pi/\omega_F$. By this time, the excitations already cascade to $k > 1/\xi$ and, while at low k their distribution is clearly anisotropic, at $k \gtrsim 1/\xi = 1.0\ \mu\text{m}^{-1}$ it is isotropic [47].

With the isotropy of the momentum distribution established for $k \gtrsim 1/\xi$ and $t \geq 2\pi/\omega_F$, we turn to TOF

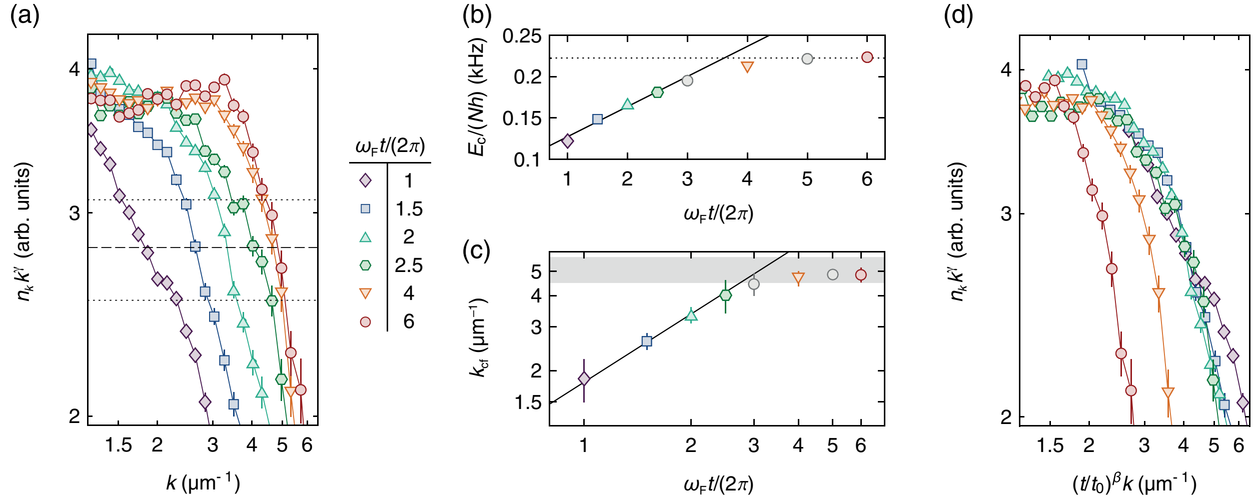

FIG. 3. Dynamic scaling in the pre-steady-state. (a) Compensated spectra $n_k k^\gamma$, with $\gamma = 2.9$; note that $1/\xi = 1.0\ \mu\mathrm{m}^{-1}$. (b) Total kinetic energy in the isotropic cascade $E_c(t)$, obtained by integrating over the spectra in (a). The slope of the solid line is equal to the independently measured flux ϵ injected at $\mathbf{k}_F$, and the horizontal dotted line is a guide to the eye. For $t \gtrsim 3.5 \times 2\pi/\omega_F$ the steady-state cascade is established. (c) The cascade front $k_{\mathrm{cf}}(t)$, defined in (a) by the intersections of the data with the horizontal dashed line; error bars show systematic uncertainties defined by the intersections with the two dotted lines. The solid line shows the prediction $k_{\mathrm{cf}} \propto t^{-\beta}$, with $\beta = -0.91$ based on Eq. (2). A fit for $t < 3 \times 2\pi/\omega_F$ (not shown) gives a consistent $\beta = -0.85(7)$. The shaded region corresponds to the independently estimated $k_D \propto \sqrt{U_D}$, including its uncertainty. (d) Compensated spectra from (a) rescaled according to Eq. (1), with $\beta = -0.85$, $\alpha = \gamma\beta = -2.47$, and the arbitrary t_0 set to $2.5 \times 2\pi/\omega_F$. Note that $(t/t_0)^{-\alpha}[(t/t_0)^\beta k]^\gamma n_k = n_k k^\gamma$, so when rescaling compensated spectra the y axis remains the same. The collapse of the curves for $t < 3 \times 2\pi/\omega_F$ shows the dynamic scaling in the pre-steady-state.

measurements to study how $n_k(k,t)$ evolves until the steady state is reached. In Fig. 3(a), we show the evolution of the compensated spectrum $n_k k^\gamma$, which highlights the propagation of its leading edge. From n_k, measured at half-periods of the drive, we extract the total kinetic energy in the isotropic cascade ($k > 1/\xi$), $E_c(t) = \int dk 2\pi k \varepsilon_k$, where $\varepsilon_k = n_k \hbar^2 k^2/(2m)$ [40] [Fig. 3(b)] and the cascade front $k_{\mathrm{cf}}(t)$ [Fig. 3(c)].

Beyond some time $t^* \approx 3.5 \times 2\pi/\omega_F$, both E_c and k_{cf} saturate, as expected for a steady state with matching energy injection and dissipation [34]. Prior to that, the growth of E_c is consistent with the independently measured ϵ injected at $\mathbf{k}_F$ (solid line); note that the systematic error in ϵ is ≈20%, dominated by the errors in the calibration of N and L (see Supplemental Material [40]). For $k_{\mathrm{cf}} > 1/\xi$, associating a constant increase of E_c with the growth of k_{cf} leads to the scaling prediction [19,33] $k_{\mathrm{cf}} \propto t^{-\beta}$ (for $t < t^*$), with

$$\beta = -1/(d + 2 - \gamma), \qquad (2)$$

where d is the system dimensionality [48]. Note that this relation assumes a quadratic wave dispersion, which is our case for $k > 1/\xi$ [49]. For a quadratic dispersion, the analytical theory of weak-wave turbulence [19,20] predicts $\gamma = d = 2$ and $\beta = -1/2$, assuming very weak interactions and $\ln(k_D/k_F) \gg 1$. Our experimental γ is different, and the origin of this difference remains to be elucidated (note that in a 3D gas $\gamma \approx 3.5$ was observed [12]). However, the relationship between β and γ in Eq. (2), which embodies the concept of dynamic scaling, should hold more generally [33], as its derivation is valid for any $\gamma < d + 2$ [19,20]. Taking our experimental $\gamma = 2.90(5)$ and $d = 2$, we predict $\beta = -0.91(4)$, and in Fig. 3(c) we show that $k_{\mathrm{cf}}(t)$ agrees with this prediction (solid line). Alternatively, fitting $k_{\mathrm{cf}} \propto t^{-\beta}$ for $t < 3 \times 2\pi/\omega_F$ gives a consistent $\beta = -0.85(7)$ (not shown), with the error dominated by the systematic uncertainty in $k_{\mathrm{cf}}(t)$.

In Fig. 3(d), we show the data from Fig. 3(a) rescaled according to Eq. (1). The collapse of the curves for $t < t^*$ confirms the dynamic scaling in the pre-steady-state, and we also show its breakdown at longer times. In the dynamics of closed quantum systems, such breakdown is expected when a system approaches equilibrium [25,28,29]; here it occurs when our driven gas reaches a nonthermal steady state.

In conclusion, our experiments provide a complete, all-scales picture of the birth of 2D wave turbulence, and our microscopic view on the far-from-equilibrium dynamics could allow many further studies. It would be interesting to vary the energy-injection scale, explore excitations above an established turbulent steady state, and study decaying turbulence [20]. In a broader context, such studies could also allow quantum simulation of the postinflationary cosmological reheating [16]. One could also search for scenarios in which the emergence of isotropy breaks down, for example, by forcing the gas through a channel between two reservoirs [50], so that turbulence forms in a moving frame.

The supporting data for this Letter are available in the Apollo repository [51].

We thank Lena Dogra, Christoph Eigen, Nir Navon, Giacomo Roati, and Henning Moritz for discussions and comments on the manuscript. This work was supported by EPSRC (Grants No. EP/N011759/1 and No. EP/P009565/1), ERC (QBox and UniFlat), STFC (Grant No. ST/T006056/1), and QuantERA (NAQUAS, EPSRC Grant No. EP/R043396/1). J. S. acknowledges support by the DFG (Grants No. 277625399 and No. EXC 2004/1-390534769) and from Churchill College (Cambridge). Z. H. acknowledges support from a Royal Society Wolfson Fellowship.

*Corresponding author.
mg850@cam.ac.uk

[1] L. F. Richardson, *Weather Prediction by Numerical Process* (Cambridge University Press, Cambridge, England, 1922).
[2] A. N. Kolmogorov, The local structure of turbulence in incompressible viscous fluid for very large Reynolds numbers, Dokl. Akad. Nauk SSSR **30**, 299 (1941).
[3] A. Obukhov, On the distribution of energy in the spectrum of turbulent flow, Dokl. Akad. Nauk SSSR **32**, 22 (1941).
[4] R. H. Kraichnan, Inertial ranges in two-dimensional turbulence, Phys. Fluids **10**, 1417 (1967).
[5] H. L. Grant, R. W. Stewart, and A. Moilliet, Turbulence spectra from a tidal channel, J. Fluid Mech. **12**, 241 (1962).
[6] M. A. Rutgers, Forced 2D Turbulence: Experimental Evidence of Simultaneous Inverse Energy and Forward Enstrophy Cascades, Phys. Rev. Lett. **81**, 2244 (1998).
[7] S. Ghashghaie, W. Breymann, J. Peinke, P. Talkner, and Y. Dodge, Turbulent cascades in foreign exchange markets, Nature (London) **381**, 767 (1996).
[8] P. A. Hwang, D. W. Wang, E. J. Walsh, W. B. Krabill, and R. N. Swift, Airborne measurements of the wavenumber spectra of ocean surface waves. Part I: Spectral slope and dimensionless spectral coefficient, J. Phys. Oceanogr. **30**, 2753 (2000).
[9] L. Sorriso-Valvo, R. Marino, V. Carbone, A. Noullez, F. Lepreti, P. Veltri, R. Bruno, B. Bavassano, and E. Pietropaolo, Observation of Inertial Energy Cascade in Interplanetary Space Plasma, Phys. Rev. Lett. **99**, 115001 (2007).
[10] L. Chomaz, L. Corman, T. Bienaimé, R. Desbuquois, C. Weitenberg, S. Nascimbène, J. Beugnon, and J. Dalibard, Emergence of coherence via transverse condensation in a uniform quasi-two-dimensional Bose gas, Nat. Commun. **6**, 6162 (2015).
[11] N. Navon, R. P. Smith, and Z. Hadzibabic, Quantum gases in optical boxes, Nat. Phys. **17**, 1334 (2021).
[12] N. Navon, A. L. Gaunt, R. P. Smith, and Z. Hadzibabic, Emergence of a turbulent cascade in a quantum gas, Nature (London) **539**, 72 (2016).
[13] S. P. Johnstone, A. J. Groszek, P. T. Starkey, C. J. Billington, T. P. Simula, and K. Helmerson, Evolution of large-scale flow from turbulence in a two-dimensional superfluid, Science **364**, 1267 (2019).
[14] G. Gauthier, M. T. Reeves, X. Yu, A. S. Bradley, M. A. Baker, T. A. Bell, H. Rubinsztein-Dunlop, M. J. Davis, and T. W. Neely, Giant vortex clusters in a two-dimensional quantum fluid, Science **364**, 1264 (2019).
[15] W. J. Kwon, G. Del Pace, K. Xhani, L. Galantucci, A. Muzi Falconi, M. Inguscio, F. Scazza, and G. Roati, Sound emission and annihilations in a programmable quantum vortex collider, Nature (London) **600**, 64 (2021).
[16] A. Chatrchyan, K. T. Geier, M. K. Oberthaler, J. Berges, and P. Hauke, Analog cosmological reheating in an ultracold Bose gas, Phys. Rev. A **104**, 023302 (2021).
[17] G. E. Falkovich, Revised universality concept in the theory of turbulence, in *Nonlinear Waves and Weak Turbulence: With Applications in Oceanography and Condensed Matter Physics* (Birkhäuser, Boston, MA, 1993), pp. 19–44.
[18] A. Monin and A. Yaglom, *Statistical Fluid Mechanics, Volume II: Mechanics of Turbulence*, Dover Books on Physics (Dover Publications, New York, 2013).
[19] V. E. Zakharov, V. S. L'Vov, and G. Falkovich, *Kolmogorov Spectra of Turbulence* (Springer, Berlin, 1992).
[20] S. Nazarenko, *Wave Turbulence* (Springer, New York, 2011).
[21] F. Family and T. Vicsek, Scaling of the active zone in the eden process on percolation networks and the ballistic deposition model, J. Phys. A **18**, L75 (1985).
[22] M. Kardar, G. Parisi, and Y.-C. Zhang, Dynamic Scaling of Growing Interfaces, Phys. Rev. Lett. **56**, 889 (1986).
[23] M. Prüfer, P. Kunkel, H. Strobel, S. Lannig, D. Linnemann, C.-M. Schmied, J. Berges, T. Gasenzer, and M. K. Oberthaler, Observation of universal dynamics in a spinor Bose gas far from equilibrium, Nature (London) **563**, 217 (2018).
[24] S. Erne, R. Bücker, T. Gasenzer, J. Berges, and J. Schmiedmayer, Universal dynamics in an isolated one-dimensional Bose gas far from equilibrium, Nature (London) **563**, 225 (2018).
[25] J. A. P. Glidden, C. Eigen, L. H. Dogra, T. A. Hilker, R. P. Smith, and Z. Hadzibabic, Bidirectional dynamic scaling in an isolated Bose gas far from equilibrium, Nat. Phys. **17**, 457 (2021).
[26] A. D. García-Orozco, L. Madeira, M. A. Moreno-Armijos, A. R. Fritsch, P. E. S. Tavares, P. C. M. Castilho, A. Cidrim, G. Roati, and V. S. Bagnato, Universal dynamics of a turbulent superfluid Bose gas, Phys. Rev. A **106**, 023314 (2022).
[27] D. Wei, A. Rubio-Abadal, B. Ye, F. Machado, J. Kemp, K. Srakaew, S. Hollerith, J. Rui, S. Gopalakrishnan, N. Y. Yao, I. Bloch, and J. Zeiher, Quantum gas microscopy of Kardar-Parisi-Zhang superdiffusion, Science **376**, 716 (2022).
[28] R. Micha and I. I. Tkachev, Relativistic Turbulence: A Long Way from Preheating to Equilibrium, Phys. Rev. Lett. **90**, 121301 (2003).
[29] J. Berges, A. Rothkopf, and J. Schmidt, Nonthermal Fixed Points: Effective Weak Coupling for Strongly Correlated Systems Far from Equilibrium, Phys. Rev. Lett. **101**, 041603 (2008).

[30] P. Christodoulou, M. Gałka, N. Dogra, R. Lopes, J. Schmitt, and Z. Hadzibabic, Observation of first and second sound in a BKT superfluid, Nature (London) **594**, 191 (2021).

[31] D. S. Petrov, M. Holzmann, and G. V. Shlyapnikov, Bose-Einstein Condensation in Quasi-2D Trapped Gases, Phys. Rev. Lett. **84**, 2551 (2000).

[32] Z. Hadzibabic and J. Dalibard, Two-dimensional Bose fluids: An atomic physics perspective, Riv. Nuovo Cimento **34**, 389 (2011).

[33] N. Navon, C. Eigen, J. Zhang, R. Lopes, A. L. Gaunt, K. Fujimoto, M. Tsubota, R. P. Smith, and Z. Hadzibabic, Synthetic dissipation and cascade fluxes in a turbulent quantum gas, Science **366**, 382 (2019).

[34] Since the energy dissipation takes the form of atoms loss, the "steady state" can be only quasisteady and the cloud is eventually depleted. However, for all the measurements in this Letter, the fractional atom loss is at most a few percent.

[35] S. R. Segal, Q. Diot, E. A. Cornell, A. A. Zozulya, and D. Z. Anderson, Revealing buried information: Statistical processing techniques for ultracold-gas image analysis, Phys. Rev. A **81**, 053601 (2010).

[36] R. Dubessy, C. De Rossi, T. Badr, L. Longchambon, and H. Perrin, Imaging the collective excitations of an ultracold gas using statistical correlations, New J. Phys. **16**, 122001 (2014).

[37] M. Kozuma, L. Deng, E. W. Hagley, J. Wen, R. Lutwak, K. Helmerson, S. L. Rolston, and W. D. Phillips, Coherent Splitting of Bose-Einstein Condensed Atoms with Optically Induced Bragg Diffraction, Phys. Rev. Lett. **82**, 871 (1999).

[38] J. Stenger, S. Inouye, A. P. Chikkatur, D. M. Stamper-Kurn, D. E. Pritchard, and W. Ketterle, Bragg Spectroscopy of a Bose-Einstein Condensate, Phys. Rev. Lett. **82**, 4569 (1999).

[39] J. Zhang, C. Eigen, W. Zheng, J. A. P. Glidden, T. A. Hilker, S. J. Garratt, R. Lopes, N. R. Cooper, Z. Hadzibabic, and N. Navon, Many-Body Decay of the Gapped Lowest Excitation of a Bose-Einstein Condensate, Phys. Rev. Lett. **126**, 060402 (2021).

[40] See Supplemental Material at http://link.aps.org/supplemental/10.1103/PhysRevLett.129.190402 for experimental methods, which also includes additional Refs. [41–45].

[41] N. Tammuz, R. P. Smith, R. L. D. Campbell, S. Beattie, S. Moulder, J. Dalibard, and Z. Hadzibabic, Can a Bose Gas be Saturated?, Phys. Rev. Lett. **106**, 230401 (2011).

[42] R. J. Fletcher, R. Lopes, J. Man, N. Navon, R. P. Smith, M. W. Zwierlein, and Z. Hadzibabic, Two- and three-body contacts in the unitary Bose gas, Science **355**, 377 (2017).

[43] I. Gotlibovych, T. F. Schmidutz, A. L. Gaunt, N. Navon, R. P. Smith, and Z. Hadzibabic, Observing properties of an interacting homogeneous Bose-Einstein condensate: Heisenberg-limited momentum spread, interaction energy, and free-expansion dynamics, Phys. Rev. A **89**, 061604(R) (2014).

[44] C. Pethick and H. Smith, *Bose–Einstein Condensation in Dilute Gases* (Cambridge University Press, Cambridge, England, 2002).

[45] N. Prokof'ev, O. Ruebenacker, and B. Svistunov, Critical Point of a Weakly Interacting Two-Dimensional Bose Gas, Phys. Rev. Lett. **87**, 270402 (2001).

[46] S. Dyachenko, A. Newell, A. Pushkarev, and V. Zakharov, Optical turbulence: Weak turbulence, condensates and collapsing filaments in the nonlinear Schrödinger equation, Physica (Amsterdam) **57D**, 96 (1992).

[47] Note that we have taken additional measurements that show that at $k = 0$ the two axial distributions are distinct [with $\bar{n}_{k,x}(0)/\bar{n}_k^{00} = 0.40(2)$ and $\bar{n}_{k,y}(0)/\bar{n}_k^{00} = 0.50(3)$] even for $t = 5 \times 2\pi/\omega_F$, when the steady state up to k_D is already established.

[48] The derivation of Eq. (2) also assumes that the high-k states are initially unoccupied, which makes a quasipure condensate a good starting point for this study.

[49] For a general power-law dispersion $\omega_k \propto k^\eta$, the relation is $\beta = -1/(d + \eta - \gamma)$.

[50] J.-P. Brantut, J. Meineke, D. Stadler, S. Krinner, and T. Esslinger, Conduction of ultracold fermions through a mesoscopic channel, Science **337**, 1069 (2012).

[51] G. Maciej, P. Christodoulou, M. Gazo, A. Karailiev, N. Dogra, J. Schmitt, and Z. Hadzibabic, Research data supporting "Emergence of Isotropy and Dynamic Scaling in 2D Wave Turbulence in a Homogeneous Bose Gas", 10.17863/CAM.89684 (2022).